POLITECNICO
MILANO 1863

SCUOLA DI INGEGNERIA INDUSTRIALE
E DELL'INFORMAZIONE

Executive Summary of the Thesis

Integrated Sensing and Communication for Future 6G Wireless Systems in the Upper Mid-Band

Laurea Magistrale in Telecommunication Engineering - Ingegneria delle Telecomunicazioni

Author: Andrea Guerrieri

Advisor: Prof. Dario Tagliaferri

Co-advisor: Prof. Marco Mezzavilla

Academic year: 2024-25

1. Introduction

The next generation of wireless networks, 6G, is set to embody a new paradigm: rather than focusing exclusively on communication, these networks will be able to actively sense and interact with their physical surroundings. A key enabling technology for this vision is **Integrated Sensing and Communication (ISAC)** [1], which aims to combine radar sensing and data communication functionalities within a single infrastructure by sharing hardware and spectral resources.

Emerging applications, such as autonomous driving and smart cities, require sensing capabilities with centimetre-level resolution. According to the formula $\Delta R = \frac{c}{2B}$, such capabilities can only be achieved using waveforms with bandwidths of several GHz. The **Upper Mid-Band** (FR3, 7-24 GHz) frequency spectrum has emerged as an ideal candidate, offering an optimal trade-off between available bandwidth and favourable propagation characteristics. However, this spectrum is far from a clean slate: it is heavily populated by incumbent services such as military radar and satellite communications, resulting in a *fragmented and non-contiguous* spectral landscape.

This thesis addresses the following research question: *How can the high-resolution sensing performance required by 6G applications be achieved using an ISAC system in a spectrally fragmented environment such as the FR3 band?* The primary objective of this work is therefore to model, analyse, and evaluate a **coherent multiband OFDM-based ISAC system**. The system is designed to turn the limitations of FR3 spectral fragmentation into an opportunity. It achieves this by coherently processing signals from the available subbands to synthesise a much wider virtual bandwidth, delivering the required high-resolution performance.

2. Methodology

To achieve the stated objectives, an end-to-end simulation framework was developed in MATLAB to model a *communication-centric* ISAC architecture. This approach is based on a *multiband Orthogonal Frequency-Division Multiplexing (OFDM) waveform*, ensuring compatibility with current and future communication standards.

2.1. Multiband Signal Model

The system's function is to accurately estimate the targets' parameters from the received scattered signal, in order to correctly detect their presence while, at the same time, providing connectivity to the UEs.
The transmitter emits an OFDM waveform structured across K non-contiguous subbands. Within each kth subband, the signal is composed of M_k symbols, each modulated onto N_k subcarriers. Then, the wave is reflected by a number of *static* targets, indicated by L, resulting in an equal number of attenuated and delayed echoes. The received *baseband* signal (i.e. dividing by $e^{j2\pi f_{c_k} t}$) for a fixed OFDM symbol has the following expression:

$$y_{BB_k}(t) = \sum_{l=1}^{L} \rho_{k,l} \sum_{n=1}^{N_k} a_{k,n} e^{j2\pi n \Delta f (t-\tau_l)} e^{-j2\pi f_{c_k} \tau_l} + w_k(t) \quad (1)$$

where $a_{k,n}$ is the data symbol, Δf is the OFDM subcarrier spacing, f_{c_k} is the carrier frequency of the k-th subband, $\rho_{k,l}$ is the complex scattering amplitude, τ_l is the round-trip delay to the l-th target, and $w_k(t)$ is the Additive White Gaussian Noise (AWGN).
The primary challenge in parameter estimation for a multiband system arises from the high-frequency carrier phase term, $e^{-j2\pi f_{c_k} \tau_l}$, contained in Eq. (1) for each subband k. In a conventional singleband system, this term would simplify to $e^{-j2\pi f_c \tau_l}$. As it does not depend on any subband index, it can be treated as a constant phase offset and absorbed entirely into the complex scattering amplitude [3]. In the multiband case, however, this phase term varies across the different subbands. Processing multiple subbands together with different phase terms causes the likelihood function to become *highly oscillatory* and *non-convex*. To analyse its effect, it can be decomposed with respect to the system's central reference frequency, $f_0 = \frac{1}{K}\sum_k f_{c_k}$, as follows:

$$e^{-j2\pi f_{c_k} \tau_l} = e^{-j2\pi f_0 \tau_l} \cdot e^{-j2\pi \Delta f_{c_k} \tau_l} \quad (2)$$

where $\Delta f_{c_k} = f_{c_k} - f_0$ is the frequency offset of each subband. While the common phase term $e^{-j2\pi f_0 \tau_l}$ can be absorbed into the complex amplitude, the second term, $e^{-j2\pi \Delta f_{c_k} \tau_l}$, introduces a destructive interference pattern that depends on the spectral gaps. These oscillations increase the energy of the sidelobes, generating numerous *local minima* in the likelihood function, which cause optimisation problems to get stuck.
Finally, the receiver extracts the Channel Impulse Response (CIR), $h(t)$, which in the case of a *monostatic* system is obtained by dividing the received signal by the known data symbols $a_{k,n}$. The oscillatory nature of the carrier phase term propagates into the CIR, which makes estimating the delays $\boldsymbol{\tau}$ non-trivial.

2.2. Parameter Estimation

In this model, the set of *parameters of interest* is given by the vector $\boldsymbol{\eta} = \{\boldsymbol{\rho}, \boldsymbol{\tau}\}$. In order to reconstruct the scattered echoes and reliably detect the presence of close-spaced targets amidst noisy observations, these parameters must be accurately estimated from the received multiband signal, as they would not be visible in a single-band one.
In signal processing, the standard approach to parameter estimation in the absence of prior knowledge is the *Maximum Likelihood Estimation (MLE)* principle. Given the observed data $\mathbf{y}$, the ML estimator $\hat{\boldsymbol{\eta}}(\mathbf{y})$ seeks the parameter set that maximises the parametric probability density function $p(\mathbf{y}|\boldsymbol{\eta})$, which represents the *likelihood* of observing the received data [2]. This maximisation problem reduce itself to a least squares minimisation. However, as discussed in Subsection 2.1, the highly oscillatory and non-convex nature of the likelihood function poses a significant challenge to direct MLE. This complex optimisation landscape renders conventional gradient-based methods ineffective and exhaustive brute-force searches computationally prohibitive. To overcome this, the thesis employs the robust iterative **Expectation-Maximisation (EM)** algorithm. To ensure its convergence to the global maximum and avoid sub-optimal local optima, the EM algorithm is initialised using the **Successive Interference Cancellation (SIC)** technique, which sequentially estimates and subtracts the contributions of the strongest targets.

2.2.1 Problem Formulation

The EM algorithm recasts the problem by defining the observed multiband CIR as the *incom-*

plete data, $\mathbf{h}$. The *complete data* is defined as the set of theoretical signals $\mathbf{y} = \{\mathbf{y}_1, \mathbf{y}_2, ..., \mathbf{y}_L\}$, where each $\mathbf{y}_l$ represents the echo from the l-th target as if it were the only one present; the fundamental relationship is that the observed signal is expressed as their sum: $\mathbf{h} = \sum_{l=1}^{L} \mathbf{y}_l$. The goal of the EM algorithm is to estimate these separated components to simplify the overall estimation of the parameters.

To derive the observation vector $\mathbf{h}$, the CIR is computed via Inverse Discrete Fourier Transform (IDFT) from the Channel Frequency Response (CFR) obtaining the sinc-like functions centered with the target delays. It is then sampled in time domain, yielding the discrete-time multiband CIR, $h[q]$, where q is the time index. A key step in the estimation model is to factorise the complex amplitude $\rho_{k,l}$ as $\rho_{k,l} = \lambda_{0_k}\rho_l$, where λ_{0_k} is the wavelength of the kth subband's carrier frequency and ρ_l is the frequency-independent complex reflectivity of the l-th target. Hence, ρ_l becomes, together with the delay τ_l, a parameter to be estimated, resulting in a total number of $2L$ parameters ($\boldsymbol{\eta} \in \mathbb{C}^{2L}$).

The resulting model for the time-sampled CIR vector $\mathbf{h} = [h[1], \ldots, h[Q]]$ is:

$$\mathbf{h} = \boldsymbol{\chi}(\boldsymbol{\tau})\boldsymbol{\rho} + \mathbf{w} \tag{3}$$

Eq. (3) shows that $\mathbf{h}$ is a linear combination of the *multiband range ambiguity functions* $\boldsymbol{\chi}(\tau_l)$, weighted by the unknown amplitudes ρ_l. Being B_k the bandwidth of the kth subband, the expression of $\chi[q](\tau_l)$ is:

$$\chi[q](\tau_l) = \sum_{k=1}^{K} \lambda_{0_k} \frac{\sin(\pi B_k(q\Delta\tau - \tau_l))}{\sin(\pi(q\Delta\tau - \tau_l))} e^{-j2\pi\Delta f_{c_k}\tau_l} \tag{4}$$

2.2.2 SIC Initialisation and EM Algorithm ($L = 2$)

The detection problem is formulated as a binary hypothesis test, in which the *alternative hypothesis*, $\mathcal{H}_1$, represents the detection of multiple targets, specifically $L = 2$. Consequently, the estimation pipeline is run to compute the parameter set $\hat{\boldsymbol{\eta}}_1 = \{\hat{\tau}_1, \hat{\tau}_2, \hat{\rho}_1, \hat{\rho}_2\}$.

As mentioned above, to ensure convergence to the global maximum, the EM algorithm is initialised via SIC. First, the parameters of the strongest target are estimated from the observation vector $\mathbf{h}$ by finding the delay that maximises the matched filter output (periodogram):

$$\hat{\tau}_1^{(0)} = \arg\max_{\tau} \frac{|\boldsymbol{\chi}^H(\tau)\mathbf{h}|^2}{\|\boldsymbol{\chi}(\tau)\|^2} \tag{5}$$

The corresponding complex amplitude is then found by projection:

$$\hat{\rho}_1^{(0)} = \frac{\boldsymbol{\chi}^H(\hat{\tau}_1^{(0)})\mathbf{h}}{\|\boldsymbol{\chi}(\hat{\tau}_1^{(0)})\|^2} \tag{6}$$

The contribution of this target is then subtracted from $\mathbf{h}$ to create a residual signal, $\mathbf{h}_{res} = \mathbf{h} - \boldsymbol{\chi}(\hat{\tau}_1^{(0)})\hat{\rho}_1^{(0)}$, and the process is repeated onto to $\mathbf{h}_{res}$ to find the initial parameters for the second target.

These initial estimates are then refined by the EM algorithm, which alternates between two steps until convergence:

E-Step (Expectation): At iteration i, an estimate of the isolated signal for each target, $\hat{\mathbf{y}}_l^{(i)}$, is computed by distributing the overall residual error. For the first target would be:

$$\hat{\mathbf{y}}_1^{(i)} = \boldsymbol{\chi}(\hat{\tau}_1^{(i)})\hat{\rho}_1^{(i)} + \frac{1}{2}\left(\mathbf{h} - \sum_{l=1}^{2} \boldsymbol{\chi}(\hat{\tau}_l^{(i)})\hat{\rho}_l^{(i)}\right) \tag{7}$$

M-Step (Maximisation): The parameters for each target are updated by performing an independent ML estimation on its separated signal component. The delay $\hat{\tau}_l^{(i+1)}$ is found by maximising the periodogram of the corresponding isolated signal, analogously to Eq. (5):

$$\hat{\tau}_l^{(i+1)} = \arg\max_{\tau_l} \frac{|\boldsymbol{\chi}^H(\tau_l)\hat{\mathbf{y}}_l^{(i)}|^2}{\|\boldsymbol{\chi}(\tau_l)\|^2} \tag{8}$$

The updated amplitudes $\hat{\rho}_l^{(i+1)}$ are then found by projection, as in Eq. (6). This iterative process continues until the parameter estimates converge. The key advantage of the EM algorithm is its ability to break down the complex, multi-target optimisation problem into simpler, single-target estimations. Rather than performing an exhaustive L-dimensional search over all possible delay combinations, which would be computationally prohibitive, the M-step only requires a simple one-dimensional search (i.e. a periodogram calculation) for each target, as shown in Eq. (8). This makes the estimation process computationally feasible.

2.3. Target Detection via GLRT

The final stage of the pipeline is to decide whether one or two targets are present, based on the parameter estimates obtained from the EM algorithm. This decision is formulated as a binary hypothesis testing problem, where the decision variable is the absolute value of the observed signal, $v = |\mathbf{h}|$, as the test involves comparing a scalar threshold γ, with another scalar. The two hypotheses translate into the following expressions:

$$v = \begin{cases} \mathcal{H}_0 : |\boldsymbol{\chi}(\tau_1)\rho_1 + \mathbf{w}| \\ \mathcal{H}_1 : |\boldsymbol{\chi}(\tau_1)\rho_1 + \boldsymbol{\chi}(\tau_2)\rho_2 + \mathbf{w}| \end{cases} \tag{9}$$

Since the parameters under each hypothesis are unknown, but they are estimated, the standard Likelihood Ratio Test (LRT) is not applicable. Instead, the **Generalised Likelihood Ratio Test (GLRT)** is employed where unknown parameters in the likelihood ratio are replaced with their respective estimates. The GLRT criteria, $\bar{\Lambda}_G(v)$, can be expressed as the ratio of the maximised likelihoods computed with the ML estimates derived from the EM algorithm under each hypothesis, i.e. $\hat{\boldsymbol{\eta}}_0$ and $\hat{\boldsymbol{\eta}}_1$. Therefore, its expression is:

$$\bar{\Lambda}_G(v) = \frac{\max_{\hat{\boldsymbol{\eta}}_1} p(v|\hat{\boldsymbol{\eta}}_1, \mathcal{H}_1)}{\max_{\hat{\boldsymbol{\eta}}_0} p(v|\hat{\boldsymbol{\eta}}_0, \mathcal{H}_0)} \underset{\mathcal{H}_0}{\overset{\mathcal{H}_1}{\gtrless}} \gamma \tag{10}$$

The decision is made by comparing this statistic to a threshold, γ, which is set to maintain a constant false alarm rate (CFAR) and it is selected such that:

$$\Pr(\bar{\Lambda}_G(v) > \gamma \,|\, \mathcal{H}_0) = P_{FA}, \tag{11}$$

where P_{FA} is the desired false alarm probability. If $\bar{\Lambda}_G(v) > \gamma$, it is decided that two targets are present ($\mathcal{H}_1$); otherwise, it is decided that only one target is present ($\mathcal{H}_0$).

3. Results

The performance of the proposed coherent multiband ISAC system was evaluated through parametric simulations. The analysis focused on the system's ability to correctly detect two closely spaced targets, evaluating the *probability of correct detection* (P_{CD}) and the *Receiver Operating Characteristic (ROC)* curves under various conditions. It also compared the ideal case where the target parameters were known beforehand with the case where the EM algorithm estimated them.

3.1. Efficacy of the Multiband

The primary finding is corroborating that a multiband approach can achieve a better resolution, thereby increasing the system's ability to distinguish between targets that would be unresolvable for a conventional single-band system. For example, a single 100 MHz subband provides a theoretical range resolution of 1.5 metres. As shown in Figure 1, this is insufficient to distinguish between two targets spaced 0.5 metres apart, resulting in a single detection. In contrast, *coherently* combining four contiguous 100 MHz subbands to form a total bandwidth of 400 MHz achieves a finer resolution of 0.375 m, clearly resolving the two distinct targets. Furthermore, *coherently* processing multiple subbands enables better performance than a single-band system with the same total bandwidth: the information contained in each subband is aligned with that in the others, resulting in constructive summation and reinforcement of the detection and outperforming the single-band system.

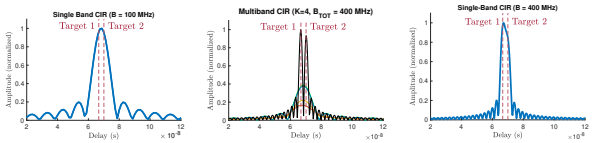

(a) SB - 100 MHz (b) MB - 400 MHz (c) SB - 400 MHz

Figure 1: CIRs of a a) single-band system of B = 100 MHz, b) multiband system of B = 400 MHz and c) single-band system of B = 400 MHz.

3.2. Trade-off of Spectral Gaps

Although spectral gaps improve theoretical resolution, they introduce a significant trade-off by creating high-energy sidelobes in the CIR. These artefacts can be misinterpreted as weaker targets and complicate the estimation process, particularly at low Signal-to-Noise Ratios (SNRs).
Consequently, detection performance does not improve monotonically with the number of subbands. Each spectral layout generates a distinct sidelobe pattern, and the system's performance depends critically on the position of true targets within this pattern. In certain configurations, a target's echo may be obscured by sidelobes,

resulting in estimation failure. Figure 2 illustrates this non-monotonic behaviour. It plots the Probability of Correct Detection (P_{CD}) versus the number of subbands (K) for two different target spacings (ΔR) at an SNR of 10 dB.
The plot shows that for a target spacing of $\Delta R = 0.5$ m (orange line), performance drops at $K = 5$. However, when the target spacing is changed to $\Delta R = 2.7$ m (blue line), the same $K = 5$ configuration performs well, while other layouts (e.g., $K = 9$) now exhibit performance degradation. This confirms that detection reliability is not solely determined by the number of subbands, but by the complex interaction between target locations and specific sidelobe interference patterns.

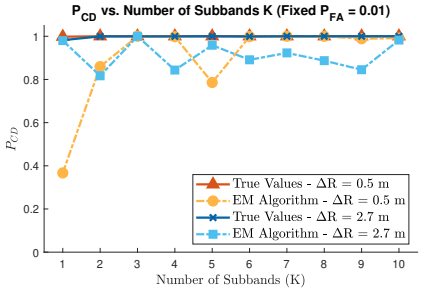

Figure 2: P_{CD} vs. Number of Subbands (K) for a fixed $P_{FA} = 0.01$ at SNR of 10 dB.

3.3. Impact of Phase Errors

A key finding of this research is that the system is highly sensitive to inter-band phase incoherence, which disrupts the coherent sum of information. In any practical implementation, hardware imperfections, such as phase noise from local oscillators and non-synchronised clocks, will introduce random phase errors between subbands. To quantify this effect, simulations were conducted that introduced random independent phase errors drawn from a zero-mean Gaussian distribution.
As shown in Figure 3, the results demonstrate severe degradation in detection performance. Even moderate phase errors (e.g., with a standard deviation of $\sigma_\phi = 5°$) cause the P_{CD} to drop and severely fluctuate. This is because the EM algorithm assumes a perfectly coherent signal model and is therefore unable to distinguish between true target echoes and destructive interference patterns caused by phase corruption. This analysis identifies phase coherence as the main requirement to the implementation of an effective multiband system.

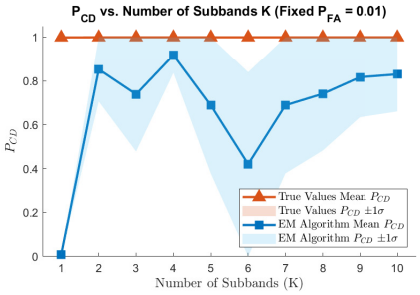

Figure 3: Average P_{CD} vs K for a fixed $P_{FA} = 0.01$ with random independent phase errors of standard deviation $\sigma_\phi = 5°$.

3.4. Feasibility with Realistic Spectrum Allocations

To validate the proposed approach in a practical context, its performance was evaluated using a realistic spectral configuration based on the World Radiocommunication Conference (WRC) allocations in FR3. The simulation employed three non-contiguous subbands spanning the 6.425-8.4 GHz range, resulting in a synthesised bandwidth of almost 2 GHz. Despite the presence of a large spectral gap of 500 MHz, the system demonstrated robust detection capabilities even at a low SNR of 5 dB. This result confirms the feasibility of leveraging real, fragmented spectrum allocations to perform high-resolution sensing effectively, provided that phase coherence can be maintained.
Further analyses were conducted to study the system's robustness under the WRC spectral configuration, focusing on the impact of the SNR and asymmetric target reflectivity (RCS).

3.4.1 Impact of SNR

As expected, the detection performance generally improves with increasing SNR. However, at very low SNR levels, the combination of the high noise floor and the strong sidelobes generated by the spectral gap makes it extremely difficult for the EM algorithm to distinguish true target echoes from spurious peaks.
Figure 4 (a) shows a counter-intuitive result at an SNR of 0 dB. The performance of the EM algorithm appears to surpass that of the case with an SNR of 2.5 dB, as well as the upper bound ROC curve computed with an ideal detector (b) with a priori knowledge of the param-

eters. This phenomenon is an artefact of the EM algorithm *overfitting* to noise, causing it to converge on noise peaks rather than the true targets. While these estimates are physically incorrect, they provide a better mathematical fit to the specific noise realisation, yielding a higher P_{CD}. The ideal detector, knowing the true target locations, correctly identifies the signal as being too weak to detect amidst the noise.

3.4.2 Impact of Different Target RCS

The system's ability to detect a weak target in the presence of a stronger one was evaluated at an SNR of 5 dB.

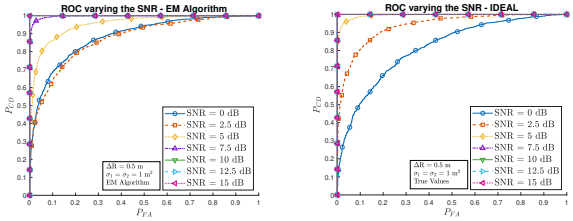

(a) ROC (SNR) - EM (b) ROC (SNR) - Ideal

Figure 4: ROC curves for the WRC configuration, varying the SNR and employing the EM algorithm (a) or the ideal detector (b).

As the RCS of the second target (σ_2) decreases, its echo becomes buried beneath the noise floor and the sidelobes of the primary target. In the simulation the RCS values are normalised, i.e. $\sigma_1 = 1$ m^2 and σ_2 is varied from 0.1 m^2 to 1 m^2. Figure 5(a) shows that for low RCS values ($\sigma_2 \leq 0.5$ m^2), the performance of the EM algorithm saturates, with the ROC curves overlapping. This is due to overfitting again: the algorithm consistently converges on the same spurious secondary peak (noise or a sidelobe) rather than the true weak target. By contrast, the performance of the ideal detector, shown in Figure 5(b), degrades progressively and accurately reflects physical reality: a target with an RCS of 0.1 m^2 is almost undetectable, with performance approaching random guessing.

4. Conclusions

This thesis has successfully demonstrated that a coherent multiband OFDM-based ISAC system is a feasible and effective solution for achieving centimetre-level sensing resolution in the fragmented 6G spectrum, FR3. The proposed methodology coherently processes information across sub-bands to exploit spectral gaps and synthesise a wider bandwidth, enabling a finer resolution and significantly better performance than conventional single-band systems.

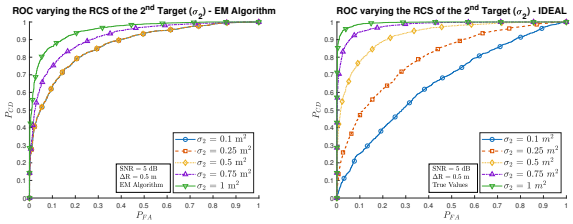

(a) ROC (RCS) - EM (b) ROC (RCS) - Ideal

Figure 5: ROC curves for the WRC configuration, varying the RCS of the second target (σ_2) at an SNR of 5 dB.

However, the study also identified two critical limitations inherent to this approach. Firstly, the spectral gaps introduce deterministic sidelobes that make the system's detection performance sensitive to the specific spectral layout. Secondly, and most critically, the system's performance depends heavily on coherent processing; without consistent phase alignment, the estimation algorithm becomes unreliable, resulting in a significant drop in detection performance.

References

[1] Fan Liu, Yuanhao Cui, Christos Masouros, Jie Xu, Tony Xiao Han, Yonina C. Eldar, and Stefano Buzzi. Integrated sensing and communications: Toward dual-functional wireless networks for 6g and beyond. *IEEE Journal on Selected Areas in Communications*, 40(6):1728–1767, 2022.

[2] Umberto Spagnolini. *Statistical Signal Processing in Engineering*. Wiley, 2018.

[3] Yubo Wan, Zhixiang Hu, An Liu, Rui Du, Tony Xiao Han, and Tony Q. S. Quek. Ofdm-based multiband sensing for isac: Resolution limit, algorithm design, and open issues. *IEEE Vehicular Technology Magazine*, 19(2):51–59, 2024.